Quantitative evaluation of mantle flow traction on overlying tectonic plate: Linear versus power-law mantle rheology

Fengyuan Cui, Zhong-Hai Li*, Hui-Ying Fu

Key Laboratory of Computational Geodynamics, College of Earth and Planetary Sciences, University of Chinese Academy of Sciences, Beijing, China

*Corresponding: li.zhonghai@ucas.ac.cn

Key Points:

- The mantle rheological flow law strongly controls the magnitude of mantle flow traction under specific geometric and kinematic conditions.
- The mantle flow traction with power-law rheology is much lower than that with linear rheology when other conditions are similar.
- The existence of continental lithospheric root can enhance the mantle flow traction by increasing both the shear and normal forces.

Abstract

The sub-plate mantle flow traction has been considered as a major driving force for plate motion; however, the force acting on the overlying plate is difficult to be well constrained. One reason lies in the variable rheological flow laws of mantle rocks, e.g. linear versus power-law rheology, applied in previous studies. Here, systematic numerical models are conducted to evaluate the mantle flow traction under variable rheological, geometrical and kinematic conditions. The results indicate that mantle flow traction with power-law rheology is much lower than that with linear rheology under the same mantle/plate velocity contrast. In addition, the existence of lithospheric root in the overlying plate enhances the mantle flow traction. In a regime with reasonable parameters, the mantle flow traction with power-law rheology is comparable to the ridge push on the order of 10^{12} N/m, whereas that with linear rheology is comparable to the slab pull of 10^{13} N/m.

Plain Language Summary

The driving force of plate motion and plate tectonics is a puzzling issue. The subducting slab pull, mid-ocean ridge push and sub-plate mantle flow traction are generally considered as three major forces, with the slab pull as the dominant one. The slab pull and ridge push are dependent on density anomaly and gravity potential, which are relatively easy for quantification. The sub-plate mantle flow traction may play critical roles in cases without slab pull and/or with limited ridge push. The mantle traction is mainly dependent on the mantle/plate velocity contrast and mantle rheology, both of which are not easy to be well constrained. Variable rheological flow laws of mantle rocks, e.g. linear versus power-law rheology, have been applied in previous studies, which may strongly affect the mantle flow traction acting on the overlying plate. Here, systematic numerical models have been conducted to quantify mantle flow traction, which indicate that the traction with power-law rheology is much lower than that with linear rheology under similar conditions. In a regime with reasonable parameters, the traction with power-law rheology is comparable to ridge push on the order of 10^{12} N/m, whereas that with linear rheology is comparable to slab pull of 10^{13} N/m.

1. Introduction

The driving force of plate tectonics is a key issue in geodynamics. It mainly includes the subducting slab pull, mid-ocean ridge (MOR) push, mantle plume forcing, as well as the traction of large-scale mantle flow beneath overlying plate (*Turcotte & Schubert*, 2002). The slab pull, generated by the negative buoyancy of cold subducting slab, is generally considered as the major driving force of plate tectonics, with the magnitude on the order of 10^{13} N/m (*Forsyth & Uyeda*, 1975). The ridge push, induced by the potential energy of elevated MOR, has the magnitude of 10^{12} N/m, i.e. one order lower than slab pull (*Turcotte & Schubert*, 2002). The mantle plume could play a significant role in the weakening of overlying lithosphere (*Baes et al*., 2020, 2021; *Gerya et al*., 2015; *van Hinsbergen et al*., 2021; *Leng & Liu*, 2023); however, its mechanical driving force may be less significant due to the point-wise character and short-time activity.

The mantle flow traction (MFT) is relatively hard to be quantitatively evaluated, due to the difficulties in constraining the mantle flow velocity relative to the overlying plate, as well as the exact viscosity and rheological model of the asthenosphere. However, the MFT may play an important role in plate tectonics, especially in the cases with missing slab pull. For example, the Tethys system experiences multiple Wilson's cycles and is characterized by multiple stages of terrane accretion, slab break-off and subduction transference (initiation), during which the slab pull is lack or absent (*Li et al*., 2023). The continued moving Tethyan chains, from southern to northern hemisphere, indicate supplementary forces are required and the MFT is a candidate (*Li et al*., 2023). The effect of MFT on plate motion has been investigated previously. For example, *Alvarez* (2010) and *Cande & Stegman* (2011) have proposed that the MFT may be a potential driving force for the long-living collision along the Himalayan belt, which is further defined as a "mantle conveyor belt" (*Becker & Faccenna*, 2011), with the MFT as high as the typical slab pull (*Li et al.*, 2022; *Lu et al.*, 2015, 2021). Meanwhile, based on the analysis of Pacific plate dynamics, *Stotz et al*. (2018) proposed that the MFT may contribute to at least 50% of the total driving forces of Pacific motion. Similarly, the mantle flow-induced driving force has been mentioned in many global

mantle convection models (*Coltice et al*., 2019; *Faccenna et al*., 2013; *Ghosh & Holt*, 2012; *Mallard et al*., 2016).

The question is about the quantitative magnitude of MFT. Can it be as high as, or even higher than, the subducting slab pull? The shear force (F_s) at the base of lithosphere in a simplest model can be expressed as:

$$F_s = \sigma_{xy} \cdot L = \eta \cdot \frac{dV_x}{dy} \cdot L \quad (1)$$

where σ_{xy} is the shear stress at the lithosphere-asthenosphere boundary (LAB), L the horizontal domain of mantle flow, η and V_x the constant viscosity and horizontal velocity of sub-plate mantle, respectively. With some typical parameters of $\eta = 10^{20}$ Pa • s, $\frac{dV_x}{dy} = \frac{2\ \mathrm{cm/yr}}{100\ \mathrm{km}}$, and L = 3000 km, the final $F_s \approx$ 1.9 TN/m, which is even lower than the normal ridge push. In this simple calculation, large uncertainties lie in the viscosity and velocity gradient of sub-plate mantle flow, both of which are dependent on the mantle rheological model. Two contrasting rheological flow laws have been applied in previous numerical models: one is the equivalent linear rheology based on the comparison with multiple large-scale geophysical observations, e.g. GIA, geoid and so on (*Billen & Gurnis*, 2001; *Mitrovica & Forte*, 2004; *Yang & Gurnis*, 2016), and the other is the power-law rheology based on laboratory experiments (e.g., *Hirth & Kohlstedt*, 2003; *Karato & Wu*, 1993; *Ranalli*, 1995). For the latter, mineral physics-based mantle rheology, the grain size has significant effect, with grain size reduction bringing effective rheological weakening (*Bercovici & Ricard*, 2012; *Foley*, 2018; *Mulyukova & Bercovici*, 2018, 2019). These contrasting rheological models can strongly affect the MFT on the overlying plate; however, the quantitative comparison and evaluation are still lacking.

In this study, systematic numerical models have been conducted to calculate the MFT with both linear and power-law rheological models. In addition, the effects of several factors, including grain size of mantle rocks, mantle/plate velocity contrast, as well as existence and thickness of lithospheric root, have been investigated to provide a more quantitative understanding of the MFT and its role in driving plate motion.

2. Numerical Method

The numerical models are conducted with the code I2VIS (*Gerya*, 2010), with specific algorithms in *Li et al*. (2019) and modifications shown in Supporting Information.

2.1. Mantle rheology

The rheological flow law of mantle rock is applied according to *Hirth & Kohlstedt* (2003):

$$\eta_{diffusion|dislocation} = \frac{1}{2}(A_H)^{-\frac{1}{n}}(\dot{\varepsilon}_{II})^{\frac{1-n}{n}} d^{\frac{p}{n}} \exp\left(\frac{E+PV}{nRT}\right) \quad (2)$$

$$\frac{1}{\eta_{ductile}} = \frac{1}{\eta_{diffusion}} + \frac{1}{\eta_{dislocation}}$$

where A_H (pre-exponential factor), n (creep exponent), p (grain size exponent), E (activation energy) and V (activation volume) are rheological parameters following *Hirth & Kohlstedt* (2003) (Table S1). Two different types of mantle rheology are compared in this study, i.e. linear (n = 1) versus power-law (n = 3.5) stress/strain rate ratio, with variable grain size (d) of 2.5 mm, 5 mm and 10 mm, respectively (*Faul & Jackson*, 2005; *Hirth & Kohlstedt*, 2003).

2.2. Model configuration

A 2D large-scale (8000 × 800 km^2) numerical model is configured (Figure S1), with a 10-km-thick sticky air layer, a 90-km-thick lithosphere and a 700-km-thick sub-lithospheric mantle in the reference case (Figure S1a). In another set of model, a thicker lithospheric root is configured in the model domain from x = 3000 to 5000 km, with the lithospheric thickness contrast of ΔH = 0 ~ 200 km (Figure S1b). In both models, permeable condition is applied on the left (influx) and right (outflux) boundaries below the bottom of lithosphere, i.e. y > 100 km in depth. Variable sub-plate mantle flow velocity relative to the stagnant overlying plate is prescribed with ΔV = 1 ~ 10 cm/yr. Contrasting effective viscosity fields are calculated under linear or power-law mantle rheology with the grain size of 5 mm in the reference model (Figure S1), in which the

mantle viscosity is consistent to the rheological profiles based on joint geophysical inversions (Figure S2). All the other parameters are shown in Supporting Information.

2.3. Calculation of mantle flow traction

The MFT acting on the overlying plate is mainly composed of two parts: shear force at the LAB and normal force at the vertical walls of lithospheric root. Thus, the MFT (F_{mft}) can be simply calculated with neglecting other minor parts:

$$F_{mft} = \int \sigma_{xy} \cdot dL + \int \sigma_{xx} \cdot dH \quad (3)$$

where σ_{xy} is the shear stress at LAB, L the length of domain for shear traction, σ_{xx} the normal stress at the vertical walls of lithospheric root, and H the depth along lithospheric root. Further on, σ_{xy} and σ_{xx} can be expressed as:

$$\sigma_{xy} = 2 \cdot \eta \cdot \dot{\varepsilon}_{xy} = \eta \cdot \left(\frac{\partial V_x}{\partial y} + \frac{\partial V_y}{\partial x} \right) \quad (4)$$

$$\sigma_{xx} = 2 \cdot \eta \cdot \dot{\varepsilon}_{xx} = 2 \cdot \eta \cdot \frac{\partial V_x}{\partial x} \quad (5)$$

where η is the effective viscosity, $\dot{\varepsilon}_{xy}$ the shear strain rate, $\dot{\varepsilon}_{xx}$ the normal strain rate, V_x and V_y the horizontal and vertical velocities of the mantle relative to overlying plate, respectively.

3. Model Result

3.1. Simple model with flat LAB

Firstly, a simple model is applied with a geometrically homogeneous overlying lithosphere (Figure 1a). Thus, the MFT is dominated by the horizontal shear force at the LAB which is represented roughly by the yellow line in Figure 1a. Dynamically, the LAB is defined as the depth where $\frac{\partial V_x}{\partial y}$ is maximum as indicated in Figures S3a and S3c for the models with linear and power-law rheology, respectively.

In the model with linear mantle rheology, the horizontal velocity gradient along *y*-axis ($\frac{\partial V_x}{\partial y}$) at the LAB increases slightly with higher ΔV (Figure 1b), whereas the vertical velocity gradient along *x*-axis ($\frac{\partial V_y}{\partial x}$) at the LAB is nearly zero (Figure S4a). Meanwhile,

the effective viscosity (η) at the LAB remains constant, if neglecting the lateral boundaries of model domain (Figure 1c). Finally, the shear stress (σ_{xy}) acting on the LAB in the central model domain increases from 0.5 MPa to around 2.5 MPa with ΔV = 1 to 5 cm/yr (Figure 1d), indicating a roughly linear correlation between shear stress and mantle/plate velocity contrast.

In the model with power-law mantle rheology, $\frac{\partial V_x}{\partial y}$ at the LAB increases greatly with higher ΔV (Figure 1e), whereas the effective viscosity decreases due to the strain-rate-dependent rheology (Figure 1f). Finally, the shear stress (σ_{xy}) acting on the LAB remains a low value from 0.25 MPa to 0.65 MPa, which is much lower than that with linear rheology (c.f. Figures 1g and 1d). It indicates that the MFT on the overlying plate is limited in the regime with power-law rheology and it cannot be increased significantly by increasing the mantle/plate velocity contrast.

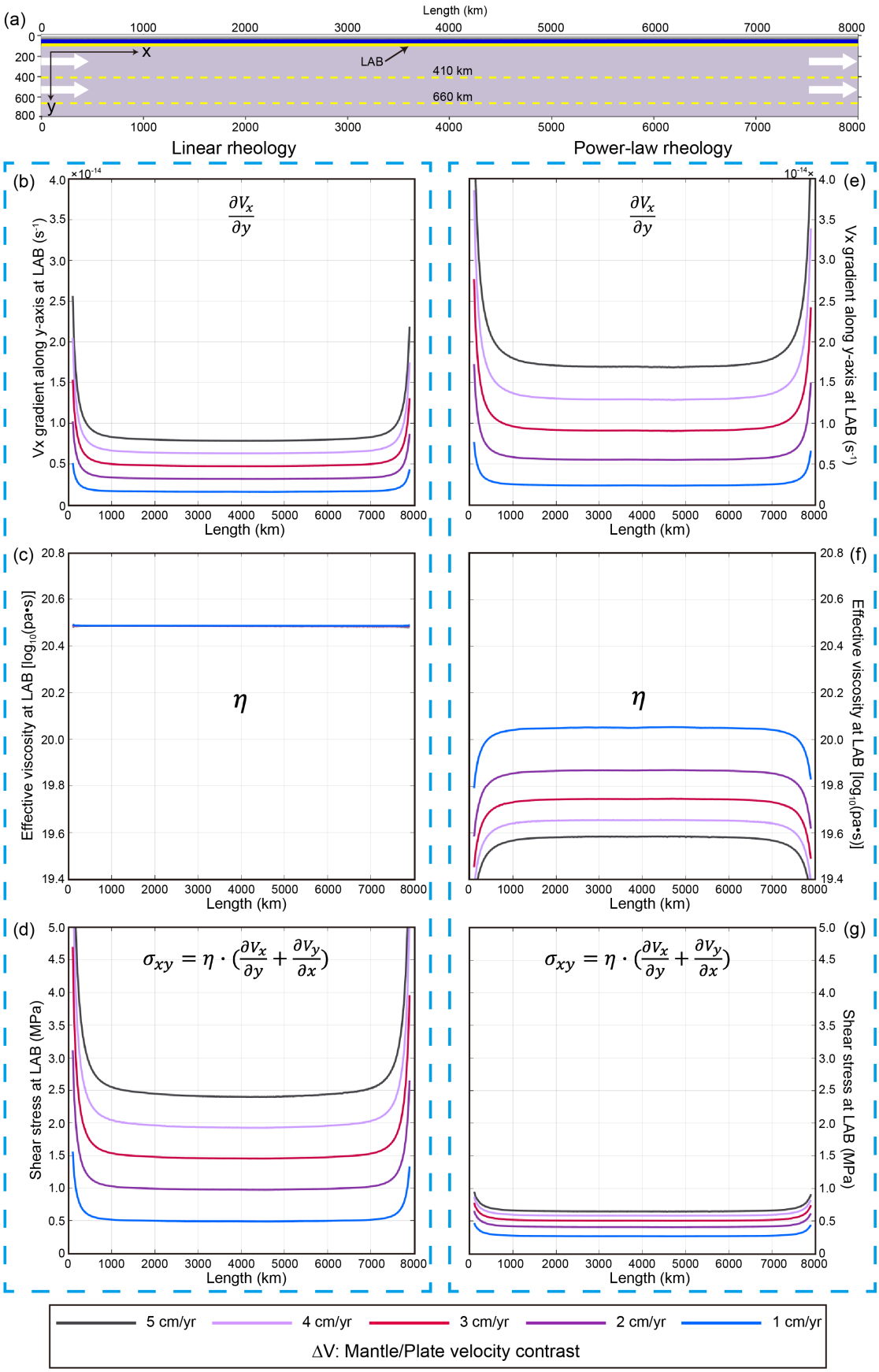
(a)
Length (km)
LAB
410 km
660 km
x
y
Linear rheology
Power-law rheology
(b)
(c)
(d)
(e)
(f)
(g)
$\frac{\partial V_x}{\partial y}$
η
$\sigma_{xy} = \eta \cdot (\frac{\partial V_x}{\partial y} + \frac{\partial V_y}{\partial x})$
Vx gradient along y-axis at LAB (s^{-1})
Effective viscosity at LAB [log$_{10}$(pa•s)]
Shear stress at LAB (MPa)
Length (km)
5 cm/yr
4 cm/yr
3 cm/yr
2 cm/yr
1 cm/yr
ΔV: Mantle/Plate velocity contrast

Figure 1. (a) Model configuration. (b-d) The calculated V_x gradient along y-axis ($\frac{\partial V_x}{\partial y}$), effective viscosity ($\eta$) and shear stress ($\sigma_{xy}$) at the LAB with linear rheology, and (e-g) with power-law rheology. Different colors represent different mantle/plate velocity contrasts (ΔV) with colorbar shown at the bottom.

3.2. Model with a lithospheric root

Since the LAB is not always flat, a lithospheric root is applied in this set of models (Figures 2-3). The MFT is composed of both shear force acting on the LAB and normal force acting on the vertical walls of lithospheric root. Dynamically, the vertical walls of lithospheric root are defined as the positions with peak $\frac{\partial V_x}{\partial x}$ values (Figure S3b, d).

Figure 2 shows the calculation of shear stress, which is more complex than that with flat LAB (c.f. Figures 2 and 1), especially in the domain of lithospheric root. However, the general trends are similar. In the models with linear rheology, the shear stress increases greatly (from 0.75 MPa to 3.5 MPa) with increasing ΔV from 1 to 5 cm/yr. In contrast, the power-law rheology results in lower shear stress (from 0.45 MPa to 1 MPa) with the same range of ΔV. Furthermore, the shear stress in the domain of lithospheric root is relatively higher, due to channel-flow-like larger velocity gradient ($\frac{\partial V_x}{\partial y}$). Again, the component of $\frac{\partial V_y}{\partial x}$ has negligible effect on the shear stress (Figure S4c-d).

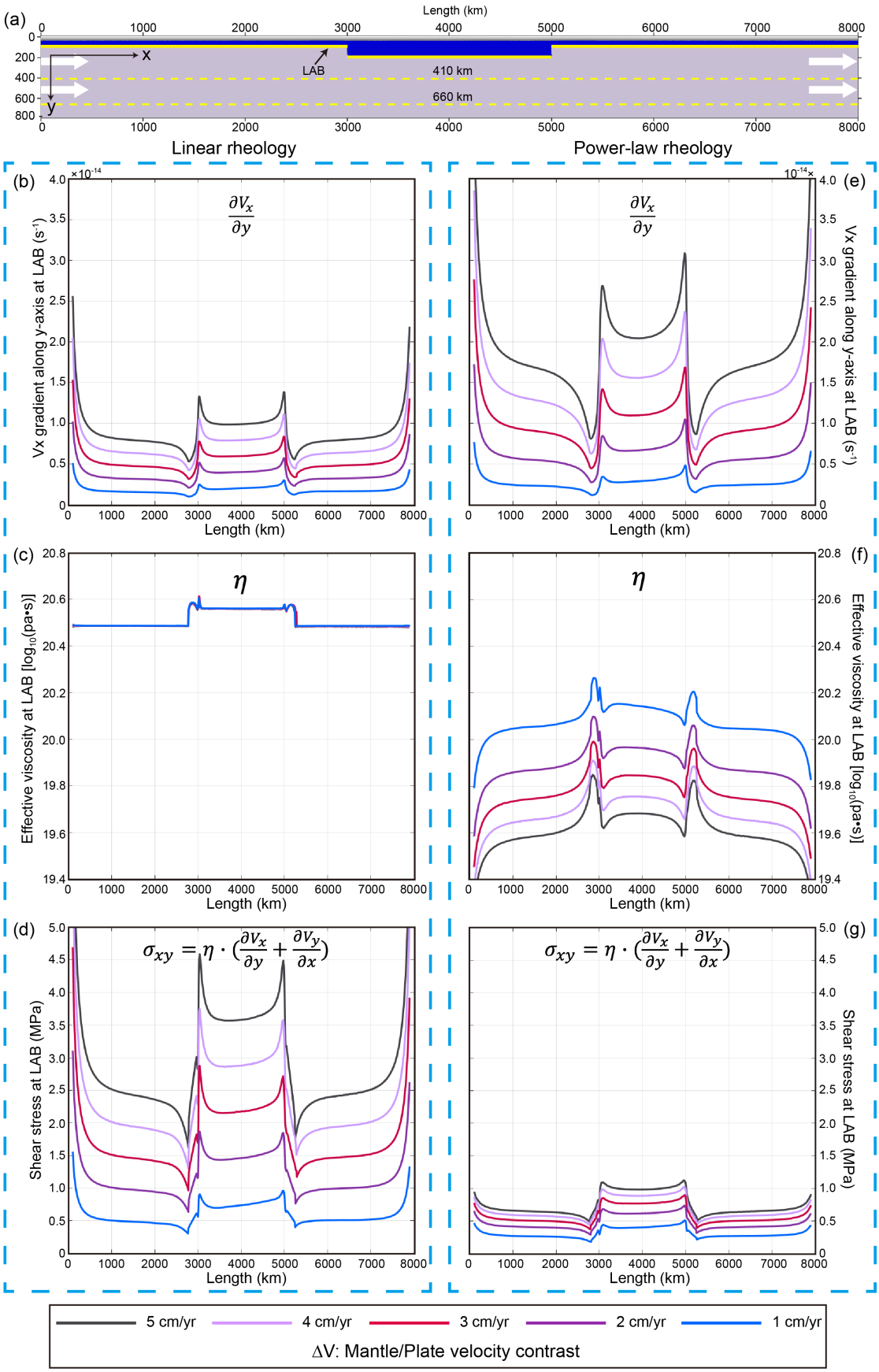
(a)
Length (km)
LAB
410 km
660 km
x
y
Linear rheology
Power-law rheology
(b)
(c)
(d)
(e)
(f)
(g)
$\frac{\partial V_x}{\partial y}$
η
$\sigma_{xy} = \eta \cdot (\frac{\partial V_x}{\partial y} + \frac{\partial V_y}{\partial x})$
Vx gradient along y-axis at LAB (s^{-1})
Effective viscosity at LAB [log$_{10}$(pa•s)]
Shear stress at LAB (MPa)
Length (km)
5 cm/yr
4 cm/yr
3 cm/yr
2 cm/yr
1 cm/yr
ΔV: Mantle/Plate velocity contrast

Figure 2. Shear stress calculation in the model with a lithospheric root of ΔH = 100 km (a) Model configuration. (b-d) The calculated V_x gradient along *y*-axis ($\frac{\partial V_x}{\partial y}$), effective viscosity ($\eta$) and shear stress ($\sigma_{xy}$) at the LAB with linear rheology, and (e-g) with power-law rheology. Different colors represent different mantle/plate velocity contrasts (ΔV) with colorbar shown at the bottom.

The normal stress at the vertical walls of lithospheric root is shown in Figure 3a-c. The normal stress at the left wall is negative, indicating compression, whereas it is positive at the right wall for extension. Thus, both of them contribute to the MFT along the positive *x* direction. Similar to shear stress, the normal stress with linear rheology is also higher than that with power-law rheology (c.f. Figures 3b and 3c). The detailed calculation routines of normal stress are shown in Figure S5.

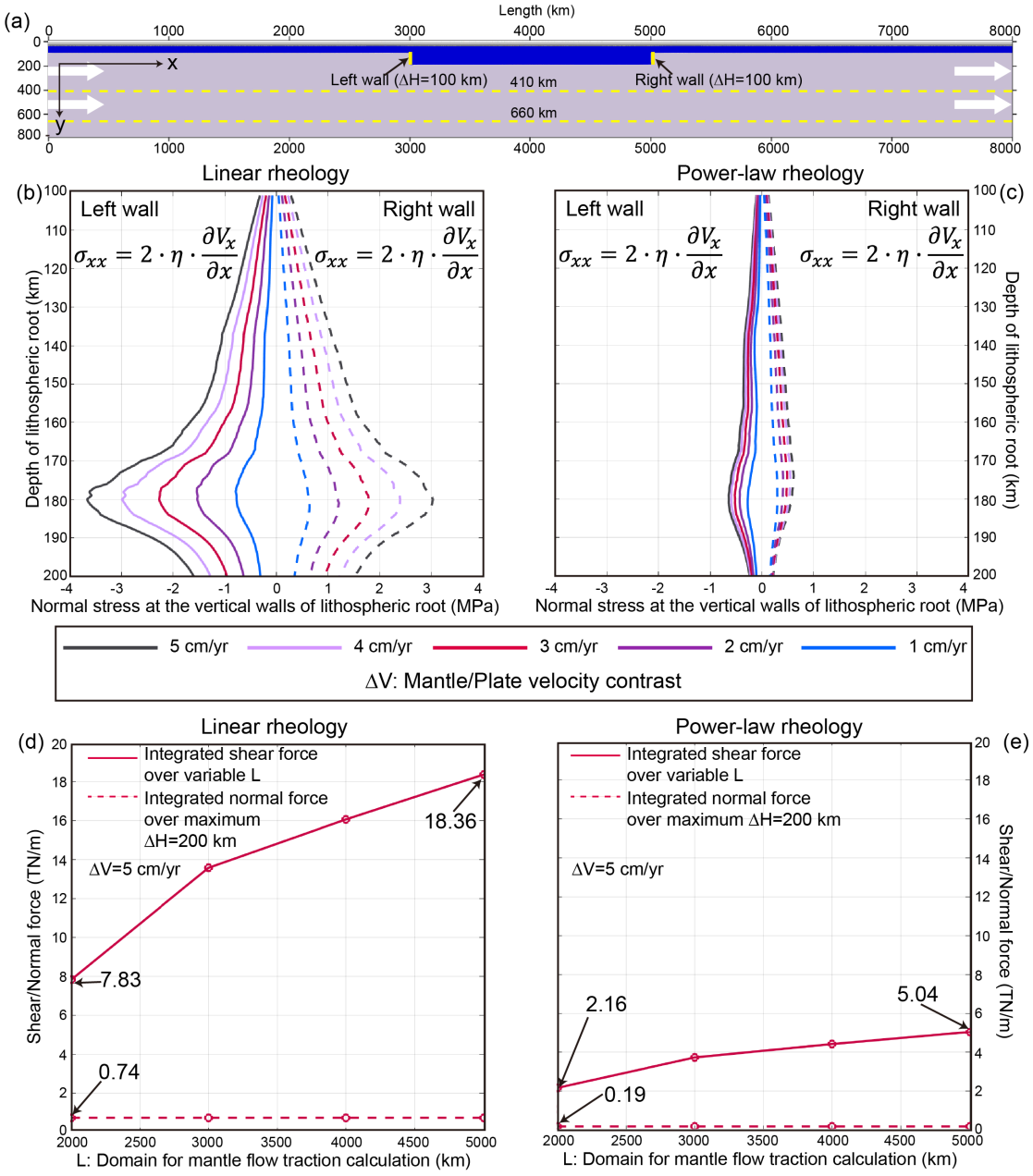

Figure 3. (a-c) Normal stress calculation at the vertical walls of lithospheric root, indicated by the yellow solid lines in (a), with either linear (b) or power-law (c) rheology. The solid and dashed lines represent the normal stress at the left and right walls, respectively. (d-e) Comparison between the integrated shear force (solid red line) over variable domain of MFT (i.e. L in the horizontal axis) and normal force (dashed red line) over a maximum thickness (ΔH = 200 km) of lithospheric root.

The comparison of shear and normal stress indicates that they have similar magnitude in the same model (c.f. Figures 2 and 3); however, the acting domain of them

could be quite different. The normal stress acts on the vertical walls of lithosphere root with a maximum ΔH of about 200 km, whereas the shear stress acts on the horizontal LAB which could be thousands of kilometers. As a direct comparison, the shear force with linear rheology ranges from 7.83 to 18.36 TN/m integrating over the length of LAB from 2000 to 5000 km, whereas the normal force is only 0.74 TN/m even with a maximum lithospheric root of ΔH = 200 km. Similarly, the shear force with power-law rheology is also much higher than the normal force. Thus, the normal stress acting on the lithospheric root could be negligible for the large-scale MFT.

3.3. Regime diagrams of mantle flow traction

The above results indicate that the MFT on overlying plate is dependent on multiple factors, including the mantle/plate velocity contrast, thickness of lithospheric root, action domain of mantle flow, as well as the mantle rheology (Figures 1-3). In order to give a systematic evaluation, two regime diagrams with the mantle flow acting domain of 3300 km (i.e. the present-day distance between northern Indian MOR and the Himalaya front) are constructed, with either linear (Figure 4b) or power-law rheology (Figure 4c). Meanwhile, the grain size, as a controlling factor for mantle viscosity, is varied between 2.5 and 10 mm (*Hirth & Kohlstedt, 2003; Karato & Wu, 1995*), with d = 5 mm as the reference value, because it produces viscosity profiles more consistent with geophysical inversions (Figure S2).

The model results indicate that the MFT with linear rheology varies from 0.22 to 62.93 TN/m in the full parameter range of ΔV = 1~10 cm/yr, ΔH = 0~200 km and d = 2.5~10 mm (Figure 4b). In the reference diagram with d = 5 mm, the traction ranges from 1.63 to 29.23 TN/m. In contrast, much lower values are predicted with power-law rheology, i.e. 0.89~5.50 TN/m, in the same range of parameters and d = 5 mm (Figure 4c). Further on, the data in the diagonal of each 2D diagram are plotted in Figure 4d. It shows clearly that the MFT increases with ΔV and ΔH; however, the value with linear rheology could be much higher than the corresponding power-law case. Thus, it is worth noting that when evaluating the MFT, it is better to identify the rheological model first.

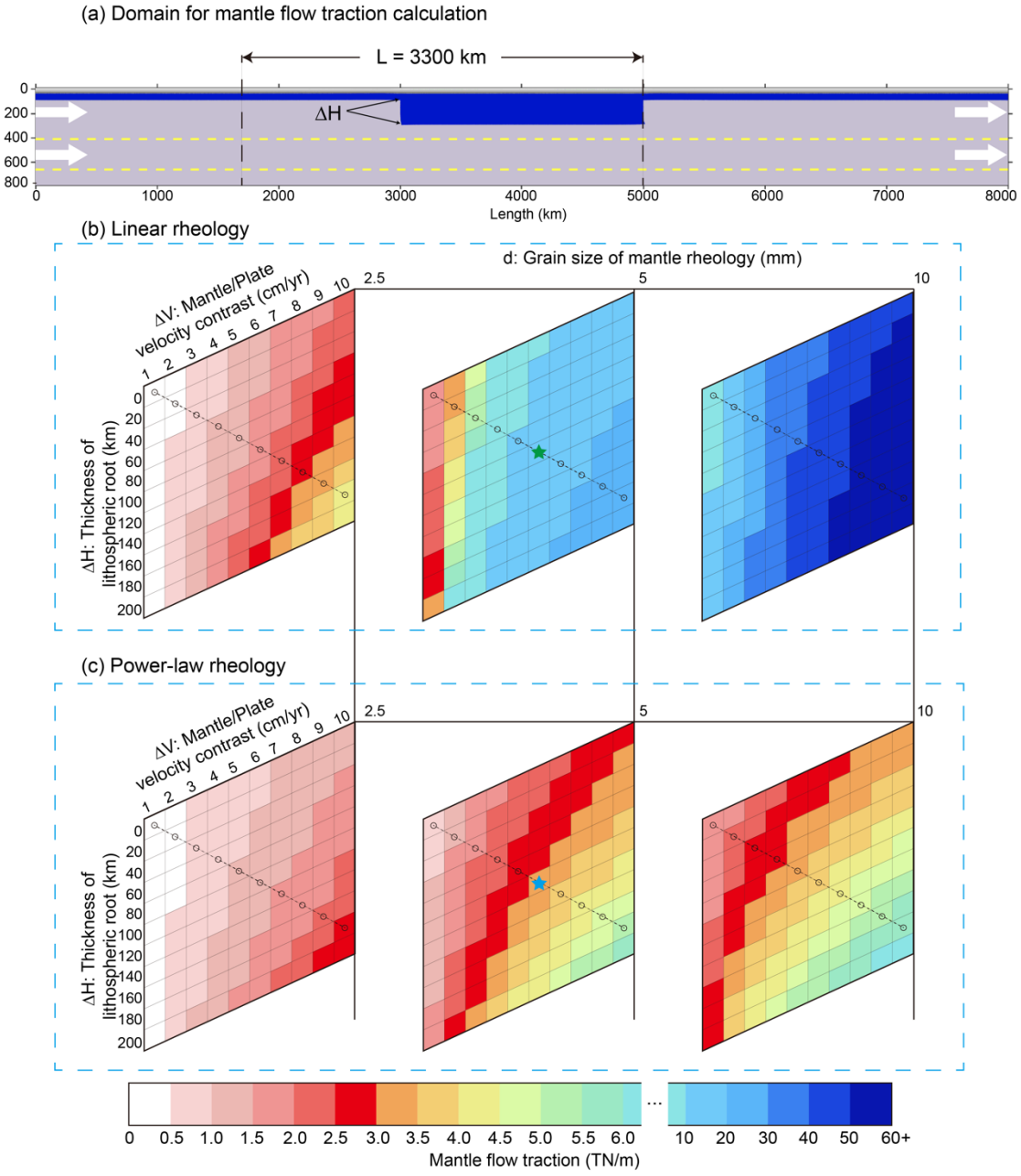
(a) Domain for mantle flow traction calculation
L = 3300 km
ΔH
Length (km)
(b) Linear rheology
d: Grain size of mantle rheology (mm)
ΔV: Mantle/Plate velocity contrast (cm/yr)
ΔH: Thickness of lithospheric root (km)
(c) Power-law rheology
Mantle flow traction (TN/m)
(d) Dependence of mantle flow traction on ΔH and ΔV along the dashed line in (b-c)
d = 2.5 mm
d = 5 mm
d = 10 mm
4.07
2.51
27.36
12.88
5.11
3.15
62.93
5.97
ΔH and ΔV increase
Linear rheology
Power-law rheology

Figure 4. (a) Domain for MFT calculation. (b-c) Phase diagram of MFT with linear and power-law rheology, respectively. The colors represent the value of MFT with the colorbar shown below. (d) Evolution of MFT with increasing thickness of lithospheric root and mantle/plate velocity contrast along the dashed lines in (b-c). The parameters and results of the 660 simulations are shown in Table S3.

4. Discussion

4.1. Effect of linear versus power-law rheology

The systematic numerical models indicate that the MFT with power-law rheology is lower than that with linear rheology in all the comparable cases with variable model configurations and numerical parameters (Figure 4, Table S3). The strain rate-induced weakening at the LAB plays a critical role in reducing the shear traction in the models with power-law rheology (Figures 1-2 and S2). Although the power-law rheology can lead to increase of velocity gradient ($\frac{\partial V_x}{\partial y}$) and thus the high strain rate at the LAB, its effect is much lower than the viscosity drop. Consequently, the latter dominates and results in the drop of MFT in the power-law rheological regime.

The effect of grain size on MFT is more significant in the linear rheological model than the power-law case (Figure 4d), because the grain size can strongly affect the diffusion part of viscous rheology (p = 3 and n = 1 in Equation 2 and Table S1), but does not change the dislocation creep (p = 0 and n = 3.5). Thus, in the regime with a larger grain size and power-law rheology, the dislocation creep dominates and the resulting MFT is limited.

On the other hand, the normal stress at the lateral walls of lithospheric root is also much lower in the power-law than the linear regime (Figures 3 and S5), with a similar mechanism of slightly increased velocity gradient but greatly decreased viscosity. It is worth noting that the walls of lithospheric root are simplified as a vertical boundary in this study, which may be more likely to be inclined. In this latter case, the normal stress may be even smaller.

4.2. Implications for the driving force of Tethyan evolution

The long-term Tethyan evolution experiences multiple Wilson cycles with repeated break-up of continental terranes from Gondwana in the southern hemisphere (Figure 5a), traveling northwards and accreting to Laurasia (Figure 5b). Then the subduction initiation occurs in the neighboring oceanic plate (Figure 5b) and continues the similar process until the final India-Asia collision (Figure 5d). During this evolution, the continental terrane collision and accretion occurs repeatedly with subducting slab break-off. In this situation with slab pull missing, the ridge push and MFT may provide the driving forces for subduction initiation. After a systematic evaluation by numerical models, *Zhong & Li* (2020) suggested that at least 8.5~9 TN/m is required for terrane collision-induced subduction transference (initiation) if no weakness exists in the passive margin. In contrast with lithospheric weakness, the subduction initiation can even occur with only ridge push of ~3 TN/m. In the former case without lithospheric weakness, the residual 5.5-6 TN/m should be provided by other sources. In the present numerical models (Figure 4), the domain for MFT calculation is 3300 km, which is about half the length scale of Paleo-Tethys and Neo-Tethys oceans, i.e. separated by the MOR (*Zhu et al.*, 2021). Based on the results, the MFT can be easily achieved/exceeded with linear rheology, whereas extreme conditions should be satisfied in order to get such a mantle traction in the power-law regime (Figure 4).

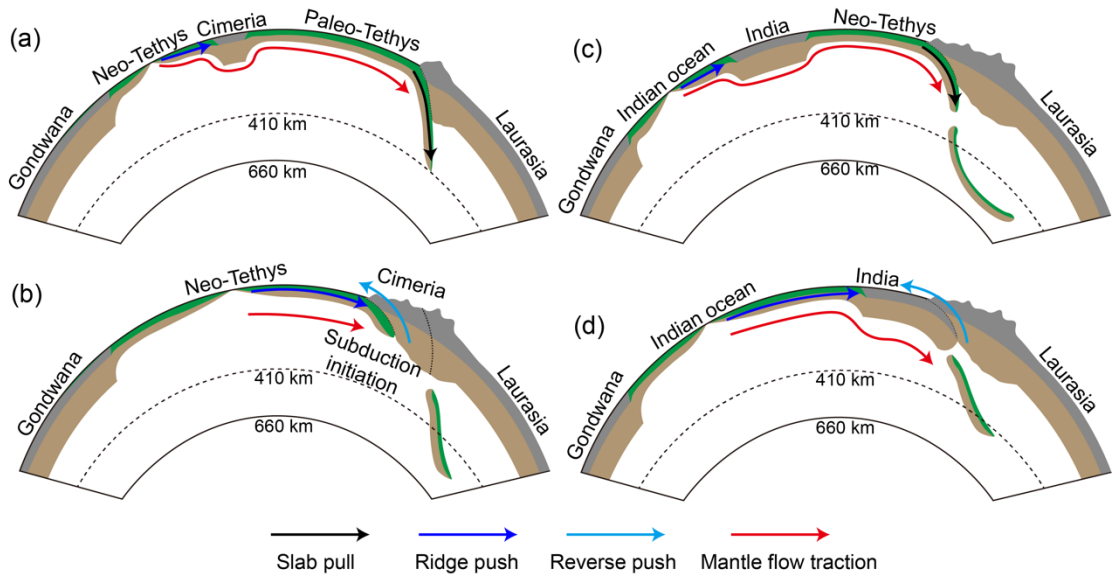

Figure 5. Key stages and possible driving forces of Tethyan evolution. (a) Paleo-Tethys subduction and Neo-Tethys spreading. (b) Collision of Cimerian terrenes with Laurasia and subduction initiation of Neo-Tethys plate. (c) Neo-Tethys subduction and Indian ocean spreading. (d) Continued collision between Indian continent and Laurasia. The arrow lines with different colors represent variable sources of driving forces.

As the final stage of Tethyan evolution, the driving force of India-Asia collision is widely debated. The present Tibetan plateau has an averaged elevation of 5 km, resulting a large push from the gravitation potential energy (GPE) of approximately 6-8 TN/m on the Indian continent and other surround terranes (*Gao et al*., 2022; *Molnar et al*., 1993). Since slab break-off occurs beneath the Tibetan Plateau, the slab pull may be negligible and hard to quantify. Another type of possible force may come from the neighboring Sumatra-Java subduction zone, with its slab pull laterally transmitted to the India-Asia collision zone (*Niu*, 2020). However, the 3D numerical models by *Zhou et al.* (2020) indicate that the lateral transmission of slab pull is dynamically difficult. A full discussion of the above forces can be found in *Li et al.* (2023). In this study, we want to test how the force of Tibetan GPE (6-8 TN/m) can be compensated by the ridge push (3 TN/m) and MFT (3-5 TN/m). The length between northern Indian MOR and Himalayan front is approximately 3300 km, as the case in Figure 4. We reasonably assume the lithospheric thickness contrast between Indian continent and Indian ocean is about 100 km. In order to get a MFT with power-law rheology of 3-5 TN/m, a mantle/plate velocity contrast should be around 6 cm/yr. Although the sub-plate mantle velocity is hard to measure directly, this value is dynamically possible and reasonable. In contrast with a linear rheology, the MFT could be much higher than required.

5. Conclusion

The MFT on overlying plate is systematically and quantitatively evaluated in this study. It indicates that the magnitude of MFT with power-law rheology is much lower than the corresponding linear rheology case. The MFT with linear rheology could be comparable to or even higher than the normal slab pull ($>10^{13}$ N/m), whereas the power-

law rheology hinders the significant increase of MFT due to the strain localization and resulting rheological weakening at the LAB depth. In addition, the existence of lithospheric root can enhance the MFT by increasing both the shear and normal stress.

The MFT could facilitate the Tethyan evolution and present-day India-Asia collision. A high mantle flow velocity and existence of lithospheric root are generally required to obtain a reasonable MFT of 3~6 TN/m in the regime with power-law rheology. In contrast, the mantle flow with linear rheology and no strain-rate weakening can easily drive any tectonic movement and deformation; the commonly considered geodynamic difficulties (e.g., subduction initiation at passive margins and long-lasting India-Asia collision) do not exist at all.

Acknowledgments

The research has received funding from the NSFC project (42225403), as well as the Fundamental Research Funds for the Central Universities. Numerical simulations were run with the cluster of National Supercomputer Center in Guangzhou (Tianhe-II) and the GeoModeling Cluster in UCAS.

Open Research

The figures of numerical models are produced by Matlab (https://ww2.mathworks.cn/products/matlab.html) and further compiled by Adobe Illustrator (https://www.adobe.com/cn/products/illustrator.html). The related data are provided in the public repository of Zenodo (https://doi.org/10.5281/zenodo.10184308).

References:

Alvarez, W. (2010). Protracted continental collisions argue for continental plates driven by basal traction. *Earth and Planetary Science Letters*, 296, 434-442. https://doi.org/10.1016/j.epsl.2010.05.030

Baes, M., Sobolv, S., Gerya, T., & Brune, S. (2020). Plume-induced subduction initiation: Single-slab or multi-slab subduction. *Geochemistry, Geophysics, Geosystems*, 21, e2019GC008663. https://doi.org/10.1029/2019GC008663

Baes, M., Sobolev, S., Gerya, T., Stern, R., & Brune, S. (2021). Plate motion and plume-induced subduction initiation. *Gondwana Research*, 98(2021), 277-288. https://doi.org/10.1016/j.gr.2021.06.007

Becker, T. W., & Faccenna, C. (2011). Mantle conveyor beneath the Tethyan collisional belt. Earth and Planetary Science Letters, 310(2011), 453-461. https://doi.org/10.1016/j.epsl.2011.08.021

Bercovici, D., & Ricard, Y. (2012). Mechanisms for the generation of plate tectonics by two-phase grain-damage and pinning. *Physics of the Earth and Planetary Interiors*, 202-203, 27-55. https://doi.org/10.1016/j.pepi.2012.05.003

Billen, M. I., & Gurnis, M. (2001). A low viscosity wedge in subduction zones. *Earth and Planetary Science Letters*, 193(2001), 227-236. https://doi.org/10.1016/S0012-821X(01)00482-4

Cande, S. C., & Stegman, D. R. (2011). Indian and African plate motions driven by the push force of the Reunion plume hear. *Nature*, 475, 47-52. https://doi.org/10.1038/nature10174

Coltice, N., Husson, L., Faccenna, C., & Arnould, M. (2019). What drives tectonic plate? *Science Advances*, 5(10), eaax4295. http://dx.doi.org/10.1126/sciadv.aax4295

Faccenna, C., Becker, T. W., Conrad, C. P., & Husson, L. (2013). Mountain building and mantle dynamics. *Tectonics*, 32(1), 80-93. http://dx.doi.org/10.1029/2012TC003176

Faul, U. H., & Jackson, I. (2005). The seismological signature of temperature and grain size variations in the upper mantle. *Earth and Planetary Science Letters*, 234(2005), 119-134. https://doi.org/10.1016/j.epsl.2005.02.008

Foley, B. J. (2018). The dependence of planetary tectonics on mantle thermal state: applications to early Earth evolution. *Philosophical transactions of the royal society A*, 376: 20170409. https://doi.org/10.1098/rsta.2017.0409

Forsyth, D., & Uyedaf, S. (1975). On the relative importance of the driving forces of plate motion. *Geophysical Journal International*, 43: 163-200. https://doi.org/10.1111/j.1365-246X.1975.tb00631.x

Gao, R., Zhou, H., Guo. X., Lu, Z., Li, W., Wang, H., et al. (2021). Deep seismic reflection evidence on the deep processes of tectonic construction of the Tibetan Plateau. *Earth Science Frontiers*, 28(5): 320-336. https://doi.org/10.13745/j.esf.sf.2021.8.10

Gerya, T. V. (2010). Introduction to numerical geodynamic modelling. Cambridge, UK: Cambridge University Press.

Gerya, T. V., Stern, R. J., Baes, M., Sobolev, S. V., & Whattam, S. A. (2015). Plate tectonics on the Earth triggered by plume-induced subduction initiation. *Nature*, 527, 221-225. https://doi.org/10.1038/nature15752

Ghosh, A., & Holt, W. E. (2012). Plate motions and stresses from global dynamic models. *Science*, 335(6070), 839-843. http://dx.doi.org/10.1126/science.1214209

Hirth, G., & Kohlstedt, D. (2003). Rheology of the upper mantle and the mantle wedge: A view from the experimentalists. *Geophysical Monograph Series*, 138, 83-105. https://doi.org/10.1029/138GM06

Karato, S., & Wu, P. (1993). Rheology of the upper mantle: A synthesis. *Science*, 260(5109), 771-778. https://doi.org/10.1126/science.260.5109.771

Leng, W., & Liu, H. (2023). Progress in the numerical modeling of mantle plumes. *Science China Earth Sciences*, 66(4):685-702. https://doi.org/10.1007/s11430-022-1058-x

Li, Y., Liu, L., Peng, D., 2022. What drives the post-collisional northward Indian motion. *American Geophysical Union Annual Meeting*, DI16A-07

Li, Z.-H., Cui, F., Yang, S., & Zhong, X. Y. (2023). Key geodynamic processes and driving forces of Tethyan evolution. *Science China Earth Sciences*, 66. https://doi.org/10.1007/s11430-022-1083-5

Li, Z.-H., Gerya, T. V., & Connolly, J. A. D. (2019). Variability of subducting slab morphologies in the mantle transition zone: Insight from petrological-thermomechanical modeling. *Earth-Science Reviews*, 196, 102874. https://doi.org/10.1016/j.earscirev.2019.05.018

Lu, G., Kaus, B. J. P., Zhao, L., & Zheng, T. (2015). Self-consistent subduction initiation induced by mantle flow. *Terra Nova*, 27, 130-138. https://doi.org/10.1111/ter.12140

Lu, G., Zhao, L., Chen, L., Wan, B., & Wu, F. Y. (2021). Reviewing subduction initiation and the origin of plate tectonics: What do we learn from present-day Earth? *Earth and Planet Physics*, 5(2), 123-140. http://dx.doi.org/10.26464/epp2021014

Mallard, C., Coltice, N., Seton, M., Muller, R. D., & Tackley, P. J. (2016). Subduction controls the distribution and fragmentation of Earth's tectonic plates. *Nature*, 535(7610), 140-143. http://dx.doi.org/10.1038/nature17992

Mitrovica, J. X., & Forte, A. M. (2004). A new inference of mantle viscosity based upon joint inversion of convection and glacial isostatic adjustment data. *Earth and Planetary Science Letters*, 225(1-2), 177-189. https://doi.org/10.1016/j.epsl.2004.06.005

Molnar, P., England, P., & Martinod, J. (1993). Mantle dynamics, uplift of the Tibetan Plateau, and the Indian Monsoon. *Reviews of Geophysics*, 31: 357-396. https://doi.org/10.1029/93RG02030

Mulyukova, E., & Bercovici, D. (2018). Collapse of passive margins by lithospheric damage and plunging grain size. *Earth and Planetary Science Letters*, 484(2018), 341-352. https://doi.org/10.1016/j.epsl.2017.12.022

Mulyukova, E., & Bercovici, D. (2019). A theoretical model for the evolution of microstructure in lithospheric shear zones. *Geophysical Journal International*, 216, 803-819. https://doi.org/10.1093/gji/ggy467

Niu, Y. (2020). What drives the continued India-Asia convergence since the collision at 55 Ma? *Science Bulletin*, 65(3), 169-172. https://doi.org/10.1016/j.scib.2019.11.018

Ranalli, G. (1995). Rheology of the earth, deformation and flow process in geophysics and geodynamics (2nd ed.). London, UK: Chapman & Hall.

Stotz, I. L., Laffaldano, G., & Davies, D. R. (2018). Pressure-driven poiseuille flow: A major component of the torque-balance governing Pacific plate motion. *Geophysical Research Letters*, 45, 117-125. https://doi.org/10.1002/2017GL075697

Turcotte, D. L., & Schubert, G. (2002). Geodynamics. Cambridge, UK: Cambridge University Press.

van Hinsbergen, D. J. J., Stein, B., Guilmette, C., Maffione, M., Gurer, D., Peters, K., et al. (2021). A record of plume-induced plate rotation triggering subduction initiation. *Nature geoscience*, 14, 626-630. https://doi.org/10.1038/s41561-021-00780-7

Yang, T., & Gurnis, M. (2016). Dynamic topography, gravity and the role of lateral viscosity variations from inversion of global mantle flow. *Geophysical Journal International*, 207(2), 1186-1202. https://doi.org/10.1093/gji/ggw335

Zhong, X. Y., & Li, Z.-H. (2020). Subduction initiation during collision-induced subduction transference: Numerical modelling and implications for the Tethyan evolution. *Journal of Geophysical Research: Solid Earth*, 125(2), e2019JB019288. https://doi.org/10.1029/2019JB019288

Zhou, X., Li, Z.-H., Gerya, T. V., & Stern, R. J. (2020). Lateral propagation-induced subduction initiation at passive continental margins controlled by preexisting lithospheric weakness. Science Advances, 6(10). https://doi.org/10.1126/sciadv.aaz1048

Zhu, R., Zhao, P., & Zhao, L. (2021). Tectonic evolution and geodynamics of the Neo-Tethys Ocean. *Science China Earth Sciences*, 65, 1-24. https://doi.org/10.1007/s11430-021-9845-7

References From the Supporting Information:

Bina, C. R., & Helffrich, G. (1994). Phase transition Clapeyron slopes and transition zone seismic discontinuity topography. *Journal of Geophysical Research*, 99(B8), 15,853–15,860. https://doi.org/10.1029/94JB00462

Bittner, D., & Schmeling, H. (1995). Numerical modeling of melting processes and induced diapirism in the lower crust. *Geophysical Journal International*, 123(1), 59-70. https://doi.org/10.1111/j.1365-246X.1995.tb06661.x

Clauser, C., & Huenges, E. (1995). Thermal conductivity of rocks and minerals. *Rock physics & phase relations*, 105-126. https://doi.org/10.1029/rf003p0105

Dziewonski, A. M., & Anderson, D. L. (1981). Preliminary reference Earth model. *Physics of the Earth and Planetary Interiors*, 25(4), 297–356. https://doi.org/10.1016/0031-9201(81)90046-7

Forte, A. M., Quere, S., Moucha, R., Simmons, N. A., Grand, S. P., Mitrovica, J. X., et al. (2010). Joint seismic-geodynamic-mineral physical modelling of African geodynamics: A reconciliation of deep-mantle convection with surface geophysical constraints. Earth and Planetary Science Letters, 295, 329-341. https://doi.org/10.1016/j.epsl.2010.03.017

Kameyama, M., Yuen, D. A., & Karato, S.-i. (1999). Thermal-mechanical effects of low-temperature plasticity (the Peierls mechanism) on the deformation of a viscoelastic shear zone. *Earth and Planetary Science Letters*, 168(1-2), 159-172. https://doi.org/10.1016/S0012-821X(99)00040-0

Karato, S.-i., Riedel, M. R., & Yuen, D. A. (2001). Rheological structure and deformation of subducted slabs in the mantle transition zone: implications for mantle circulation and deep earthquakes. *Physics of the Earth and Planetary Interiors*, 127(1-4), 83-108. https://doi.org/10.1016/S0031-9201(01)00223-0

Katayama, I., & Karato, S.-i. (2008). Low-temperature, high-stress deformation of olivine under water-saturated conditions. *Physics of the Earth and Planetary Interiors*, 168(3-4), 125-133. https://doi.org/10.1016/j.pepi.2008.05.019

Katz, R. F., Spiegelman, M., & Langmuir, C. H. (2003). A new parameterisation of hydrous mantle melting. *Geochemistry, Geophysics, Geosystems*, 4(9), 1073. https://doi.org/10.1029/2002gc000433

Kirby, K., & Kronenberg, A. K. (1987). Rheology of the lithosphere: Selected topics. *Reviews of Geophysics*, 25(6), 1219-1244. https://doi.org/10.1029/RG025i006p01219

Li, Z.-H., Liu, M., & Gerya, T. (2016). Lithosphere delamination in continental collisional orogens: A systematic numerical study. *Journal of Geophysical Research: Solid Earth*, 121(7), 5186-5211. https://doi.org/10.1002/2016JB013106

Schmidt, M. W., & Poli, S. (1998). Experimentally based water budgets for dehydrating slabs and consequences for arc magma generation. *Earth and Planetary Science Letters*, 163(1-4), 361–379. https://doi.org/10.1016/S0012-821X(98)00142-3